Original Article

Journal of Intelligent Material Systems and Structures

Journal of Intelligent Material Systems and Structures
2014, Vol 25(2) 155–163

DOI: 10.1177/1045389X13489363
jim.sagepub.com
SAGE

Precise positioning and active vibration isolation using piezoelectric actuator with hysteresis compensation

Adrien Badel, Ronan Le Breton, Fabien Formosa, Snoussi Hanene and Jacques Lottin

Abstract

This article investigates precise positioning at the micrometer scale using piezoelectric actuators. A special focus is given to the rejection of ambient vibration disturbances. An original experimental setup composed of two superposed piezoelectric actuator stages is used to evaluate the performances of the proposed approach. The bottom one is devoted to the disturbance generation, whereas the upper one allows position tracking and active stabilization. The experimental dynamic and hysteretic characterizations of the top actuator are performed. Based on the identified dynamic model, a linear controller is designed. Its performances are improved with a hysteresis compensation method. Such methods usually imply either simple symmetrical hysteresis (e.g. General Maxwell Slip) or operators able to model asymmetric loops (e.g. Preisach) at the cost of more memory usage and computational time. In the present study, a previously published lightweight asymmetric operator hysteresis is successfully used for the first time within a piezoelectric positioning closed-loop control.

Keywords

Piezoelectric actuator control, vibration isolation, hysteresis modeling and compensation

Introduction

Piezoelectric actuators (PEAs) are commercially available and widely used for micropositioning applications in the range of nanometers to micrometers (Mayhan et al., 2000; Seo et al., 2008). For high-accuracy positioning and tracking systems, the piezo-actuated system has to be equipped with a controller. The positioning accuracy is mainly affected by (1) the nonlinear hysteresis effect exhibited in ferroelectric materials and (2) the ambient vibration disturbances. Effective controllers aim at lessening these two issues. Although several methods have been proposed to model the hysteresis behavior in order to improve the control of PEAs, the effect of the vibration disturbances has hardly been studied yet.

In recent years, several methods have been proposed to develop an inverse model of hysteresis to linearize the PEA behaviors. Most of these inverse models are based on a Preisach-type model of hysteresis (Cao and Yang, 2012; Ge and Jouaneh, 1995; Jang et al., 2009; Song et al., 2005), the generalized Maxwell slip (GMS) operator (Badel et al., 2007; Goldfarb and Celanovic, 1997), the Prandtl–Ishlinskii hysteresis operator (Kuhnen and Janocha, 1999; Shan and Leang, 2012), or the Bouc–Wen model (Trabia et al., 2011; Wang et al., 2010).

The Preisach model is a very generic model of hysteresis that can represent complex asymmetric hysteretic loops. Its main drawbacks are a notched response and a large number of parameters whose identification requires numerous complex evaluations.

The GMS as well as the Prandtl–Ishlinskii or the Bouc–Wen models are quite simple and easy to implement in a real-time controller. However, their main weakness is that only central symmetric hysteresis loops can be accounted for, whereas the hysteresis loops between the voltage and the displacement of many PEAs are slightly asymmetric. To overcome this limitation, some enhanced models have been proposed, such as a modified Prandtl–Ishlinskii operator (Kuhnen,

Laboratoire Systèmes et Matériaux pour la Mécatronique, Université de Savoie, Annecy le Vieux, France

Corresponding author:
Adrien Badel, Laboratoire Systèmes et Matériaux pour la Mécatronique, Université de Savoie, Domaine universitaire, BP 80439, 74944 Annecy le Vieux, France.
Email: adrien.badel@univ-savoie.fr

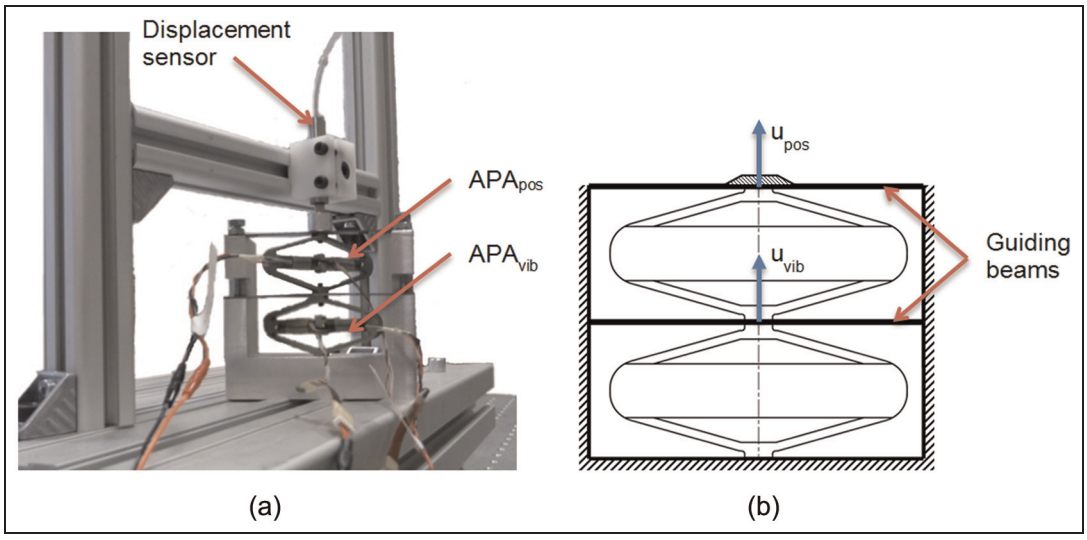

Figure 1. Experimental setup: (a) picture and (b) schematic.
APA: amplified piezoelectric actuators.

2003) and generalized Bouc–Wen models (Song and Der Kiureghian, 2006; Trabia et al., 2011), where nonsymmetrical nonlinearities have been added.

Another hysteresis operator has been recently proposed (Badel et al., 2008a, 2008b). It is able to model asymmetric hysteresis loops and is much simpler than the Preisach model. It is defined by two hyperbola functions, each of them described by three parameters only, which makes it a lightweight operator. It is not as generic as the Preisach operator but is applicable and relevant in most of the PEA operating conditions.

The use of this lightweight inverse hysteresis operator (LIHO) in the case of positioning closed-loop control has not been investigated in the literature yet. In this article, a PEA controller including the LIHO for linearization purpose is proposed.

Once the actuator behavior has been linearized, the ambient vibration disturbance rejection is to be dealt with. To the author's knowledge, this problem has been hardly studied. In this work, the disturbances are purposefully generated by an original superposed architecture.

The setup designed to produce the appropriate disturbances and to test the proposed control scheme is described in section "Experimental setup." Section "Modeling and identification" is devoted to the modeling and the identification of the system. The proposed controller is described in section "Controller design." The hysteresis effect is compensated by the LIHO, and the linear controller is designed by a loop-shaping procedure. Finally, an excellent agreement between simulations (see section "Simulation") and experimental results (see section "Experimental results"), for both the frequency and the temporal domains, demonstrates that canceling the hysteresis effect drastically improves the performances.

Experimental setup

This section describes the experimental setup used to assess the precise positioning with ambient vibration disturbance rejection using PEAs (see Figure 1). It is made by superposing two amplified piezoelectric actuators (APA 100M) from Cedrat Technologies©. Each of these actuators is driven by a voltage ranging between −20 and 150 V through a power amplifier (Cedrat technologies LA75B). Their maximal blocked force is about 180 N, their maximal free displacement is approximately 110 μm, and their clamped-free first resonance frequency is 1.9 kHz. The bottom actuator (APA$_{vib}$) generates the disturbance vibrations. The displacement u_{vib} simulates any ambient motion. It is obtained by driving the actuator APA$_{vib}$ using a voltage waveform replicating the ambient vibrations. The upper actuator (APA$_{pos}$) allows the micropositioning while compensating the forced disturbances. This stage serves both as an active positioning and as an isolating device. The displacement u_{pos} is the displacement that is to be controlled, whereas the elongation Δu of APA$_{pos}$ is the difference between u_{pos} and u_{vib}. Two flexible clamped–clamped beams are used to ensure vertical z-axis motions. Their stiffness is small enough, so that the maximal displacements generated by the actuators are practically unchanged compared with the free load case. The absolute position of the upper stage (u_{pos}) is measured by a capacitive sensor at a submicrometer resolution (Lions Precision©C23-C).

Modeling and identification

The design of the controller requires a precise modeling of the electromechanical behavior of the system. The full model of the PEA is given by a Preisach hysteresis model in series with its dynamic transfer function, as

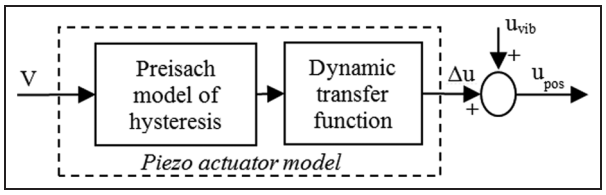

Figure 2. PEA model.
PEA: piezoelectric actuator.

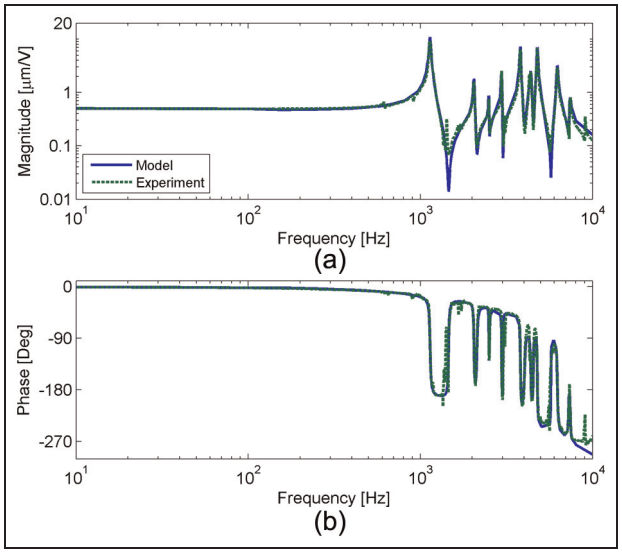

Figure 3. Comparison of experimental and identified frequency responses (small signal): (a) magnitude vs frequency and (b) phase vs frequency.

shown in Figure 2. A two-step identification procedure is proposed. First, a small signal dynamic characterization is performed and leads to the open-loop transfer function between the APA_{pos} driving voltage V and the elongation Δu (step A). Then, the piezoelectric hysterical behavior is measured at low frequency, allowing its model parameters to be identified (step B).

Dynamic transfer function identification

The experimental frequency response is obtained by driving the control stage APA with a low amplitude voltage (1 Vpp (peak-to-peak voltage)), so that the hysteresis effect can be neglected. The response is measured by the capacitive sensor. An automated procedure is performed using dSpace© real-time environment: A sinusoidal voltage is generated with a frequency ranging from 5 Hz to 10 kHz while the acquisition system sampling time is set to 10 µs. The obtained experimental actuator frequency response is shown in Figure 3.

The identification is performed using MATLAB software in order to get an accurate linear model in a wide frequency range (from DC to 10 kHz). The identification method used for parameter estimation is an adaptive version of subspace Gauss–Newton approach, suggested by Ninness et al. (2005). The obtained 19th-order model exhibits nine complex conjugate poles corresponding to nine resonances (see Table 1) and one real pole, which is due to the sensor cutoff frequency at 16 kHz ($\omega_S = 100$ krad/s). Its numerator is composed of eight complex conjugate zeros related to the antiresonances intercalated with the resonances (see Table 2). The identified transfer function is finally given by equation (1), where G_S is the static gain, evaluated to 0.48 µm/V

$$F(p) = \frac{\Delta u(p)}{V(p)} = \frac{G_S}{\left(1 + \frac{p}{\omega_S}\right)} \frac{\prod_{i=1}^{8} \left(1 + \frac{2\xi_{ia}}{\omega_{ia}} p + \frac{p^2}{\omega_{ia}^2}\right)}{\prod_{i=1}^{9} \left(1 + \frac{2\xi_{ir}}{\omega_{ir}} p + \frac{p^2}{\omega_{ir}^2}\right)} \quad (1)$$

Hysteresis model

The actuator hysteresis behavior is modeled by a classical Preisach-type model. It is worth to note that this Preisach model will not be used in the controller, but only for simulation purposes, to get a reference model of the PEA. It consists in weighted combinations of relay hysterons in parallel. This model requires $n \times (n-1)/2$ parameters, where n is the numbers of steps describing half of the major loops (see Figure 4). An automated method was used to perform identification, and a total of 4950 parameters were identified to get an accurate precision for this experimental setup ($n = 100$). A low frequency excitation (10 Hz) allowed the dynamic effects (resonances and antiresonances) to be

Table 1. Nine identified resonances.

f_{ir} (Hz)	1137	2047	2499	2963	3807	4375	4776	6244	7405
ω_{ir} (rad/s)	7145	12,859	15,703	18,615	23,920	27,486	30,009	39,232	46,530
ξ_{ir}	0.010	0.007	0.003	0.003	0.005	0.011	0.006	0.009	0.008

Table 2. Nine identified antiresonances.

f_{ia} (Hz)	1459	2132	2518	3020	4032	4535	5734	7284
ω_{ia} (rad/s)	9169	13,398	15,823	18,976	25,335	28,496	36,030	45,765
ξ_{ia}	0.008	0.010	0.004	0.003	0.014	0.008	0.004	0.010

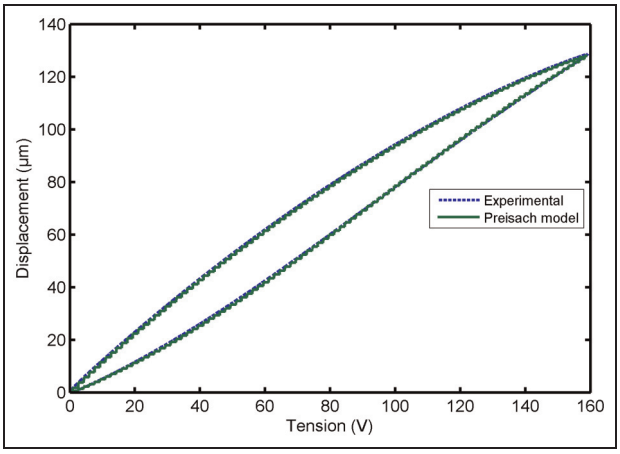

Figure 4. Experimental and Preisach models for the hysteresis loop of the actuator.

neglected. A total of n experimental loops of increasing amplitudes had to be recorded to identify the parameters, using the procedure fully described by Ge and Jouaneh (1995).

Controller design

Preliminary considerations

Because the system exhibits numerous and close resonance and antiresonance frequencies, it is not possible to efficiently reduce the order of the model. Considering that only the displacement of the top side of the control stage is measured, an accurate estimation of the system states is unfeasible. Consequently, the state space approach is discarded in favor of the loop shaping using a classical proportional–integral (PI) controller in series with a dedicated filter, as shown in Figure 5. In a first approach, the system is supposed to be linear, modeled by the transfer function identified in section "Dynamic transfer function identification." u_{ref} is the desired (or reference) displacement.

Filter design

A dedicated sixth-order filter is used to shape the open-loop system frequency response: It is composed of a notch filter in series with a fourth-order low-pass filter. The former is used to compensate the first resonance of the model, whereas the latter is added to attenuate the higher resonances (given in Table 1), thus preventing instabilities in the closed-loop system. Increasing the low-pass filter order would increase the gain margin but at the same time decrease the phase margin. Decreasing its order would have the opposite effect. The fourth order was found to be the best compromise.

The transfer function of the notch filter is given by equation (2), whose parameters are detailed in Table 3

$$H_{\text{notch}}(p) = \frac{1 + \frac{2\xi_1}{\omega_{\text{P}}}p + \frac{p^2}{\omega_{\text{P}}^2}}{1 + \frac{2\xi_2}{\omega_{\text{P}}}p + \frac{p^2}{\omega_{\text{P}}^2}} \tag{2}$$

The low-pass filter is composed of two low-pass second-order Butterworth filters in series, whose transfer function is given by equation (3)

$$H_{\text{Butter}}(p) = \frac{1}{1 + \frac{\sqrt{2}}{\omega_{\text{P}}}p + \frac{p^2}{\omega_{\text{P}}^2}} \tag{3}$$

The effect of this sixth-order filter on the open-loop frequency response is shown in Figure 6. It is clear that mechanical resonances are damped and are constantly lower than the static gain.

PI controller tuning

The PI controller's transfer function is given by equation (4), where K_{P} and K_{I} are the proportional and integral gains, respectively

$$C(p) = K_{\text{P}} + \frac{K_{\text{I}}}{p} \tag{4}$$

The control action is designed according to the following requirements: The focus is both on the response bandwidth, that is, DC to at least 100 Hz, and on the disturbance rejection, where perturbations below 100 Hz should be rejected.

The optimal control parameters, given in Table 3, are obtained by loop shaping. The gain margin and phase margin are 12.9 dB and 69.4°, respectively, as shown in Figure 7, ensuring a robust stable controlled system. The closed-loop system step response is shown in Figure 8. The position tracking matches the

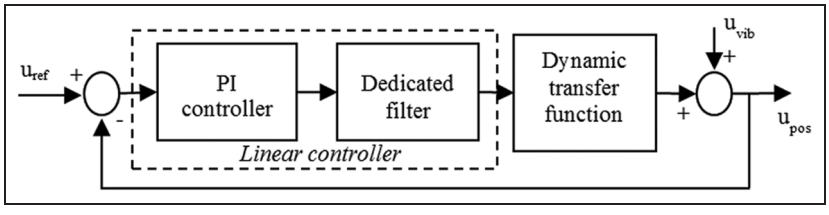

Figure 5. Block diagram of the linear controller/linear model.
PI: proportional–integral.

Table 3. Linear controller parameters.

Notch	ω_P = 7150 rad/s, ξ_1 = 0.10, ξ_2 = 0.56
First Butterworth	ω_P=8170 rad/s
Second Butterworth	ω_P=12,600 rad/s
K_P	0.0488
K_I	1820

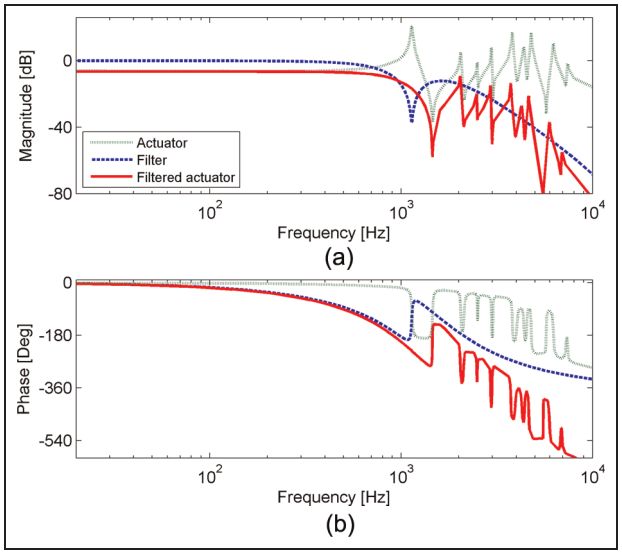

Figure 6. Comparison of open-loop system (dotted line), sixth-order filter (dashed line), and system with filter (plain line) frequency responses: (a) magnitude vs frequency and (b) phase vs frequency.

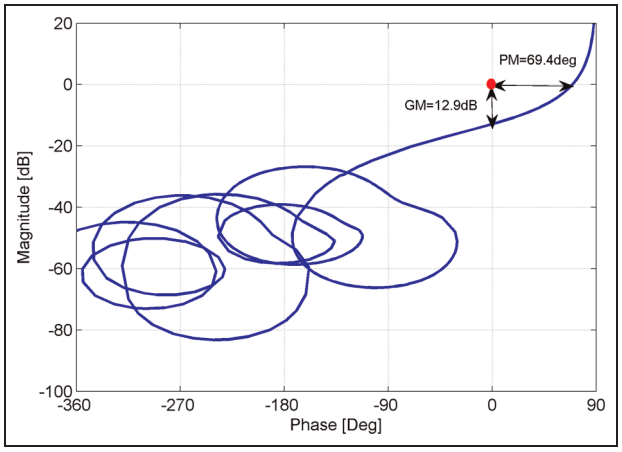

Figure 7. Black–Nichols diagram of the linear control scheme. GM: gain margin; PM: phase margin.

requirement with a settling time within 2% of 2.56 ms and a 10%–90% rise time of 1.35 ms.

The position tracking transfer function (u_{pos}/u_{ref}) and the output sensitivity (u_{pos}/u_{vib}) frequency response

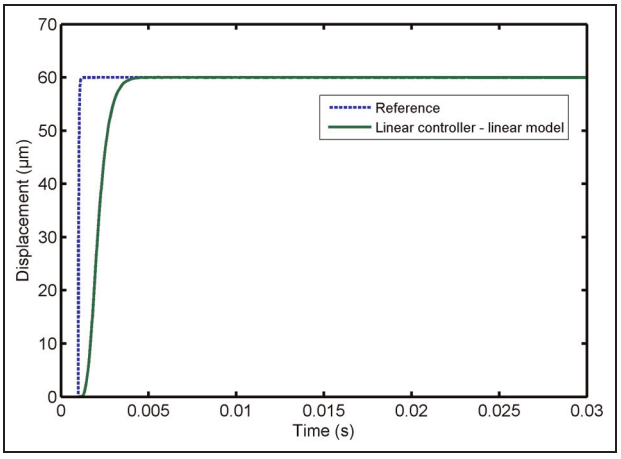

Figure 8. Response of the closed-loop linear system for a 60-µm step reference (u_{ref}).

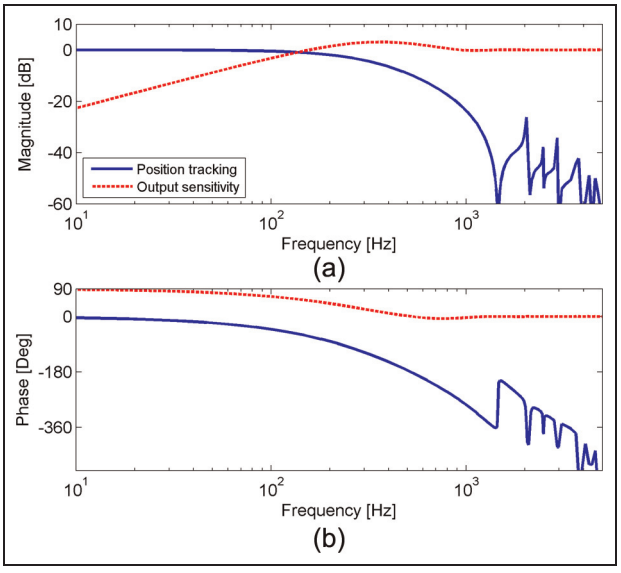

Figure 9. Comparison of position tracking (u_{pos}/u_{ref}) and output sensitivity (u_{pos}/u_{vib}) frequency responses: (a) magnitude vs frequency and (b) phase vs frequency.

are shown in Figure 9. In the frequency band from DC to 100 Hz, a flat position tracking response combined with an efficient disturbance rejection (−3.3 dB at 100 Hz) is clearly exhibited.

Linearization—hysteresis compensation

The nonlinearities induced by the hysteresis effects in PEAs may lead to unexpected overshoots and oscillations if not taken into account during the controller design. A first strategy to handle this issue is to slow down the controller, another one is to compensate the hysteresis effect using an inverse hysteresis operator added in the controller.

Table 4. Identified inverse hysteresis operator parameters.

a_1 (V)	12.6766
b_1 (μm)	12.2678
c_1 (V/μm)	2.1721
a_2 (V)	62.7439
b_2 (μm)	47.0193
c_2 (V/μm)	2.1804

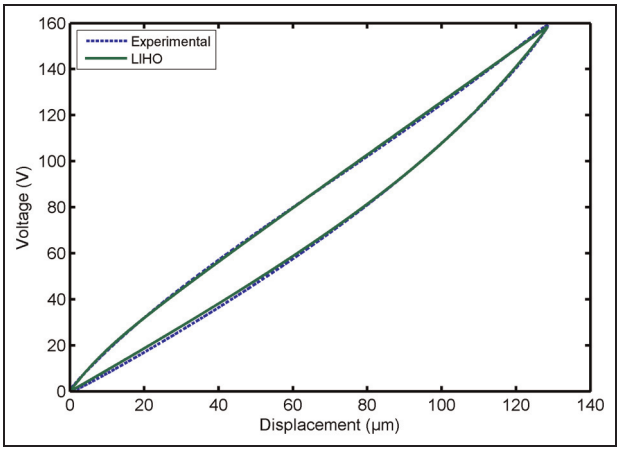

Figure 10. Experimental and LIHO loops.
LIHO: lightweight inverse hysteresis operator.

In this study, the second approach is chosen using the LIHO fully described in a previous work (Badel et al., 2008a). The main advantages of it are that it can model not centrally symmetric loops and that it only requires six parameters. It is based on the two functions defined by the equation (5): the "general ascending function"$f_1(x)$ and the "general reversal function"$g_2(x)$.

The underlying assumption of the proposed inverse hysteresis operator is that any ascending branch is a particular translation of $f_1(x)$ and that any reversal branch is a particular translation of the function $g_2(x)$

$$\begin{cases} f_1(x) = a_1\left(1 - \sqrt{1 + \frac{x^2}{b_1^2}}\right) + c_1 x \\ g_2(x) = -a_2\left(1 - \sqrt{1 + \frac{x^2}{b_2^2}}\right) + c_2 x \end{cases} \quad (5)$$

The ascending and the reversal branches are switched each time the input of the inverse hysteresis operator (i.e. the displacement) reaches an extremum. When a minimum of the displacement occurs, the hysteresis operator switches from a reversal branch to an ascending branch, and conversely, when a maximum of the displacement occurs, it switches from an ascending branch to a reversal branch.

The identified parameters are given in Table 4, and Figure 10 shows a comparison between an experimental hysteresis loop and the corresponding loop obtained through the LIHO.

Simulation

Simulations have been performed using MATLAB/Simulink software, in order to test the closed-loop tracking response and the disturbance rejection. The PI controller, the filters, and the LIHO are discretized with a sampling time of 20 μs, considering that they will later be implemented in a real-time digital system.

The block diagram of the closed-loop system is shown in Figure 11. The upper stage of the mockup is simulated by the Preisach model of hysteresis identified in section "Hysteresis model," which is in series with the linear transfer function identified in section "Dynamic transfer function identification."

In order to underline the importance of the inverse hysteresis operator in the controller design, a comparison is proposed in Figure 12 between the controllers with and without the LIHO, called "nonlinear controller" and "linear controller," respectively. A step response followed by a step disturbance is simulated in both cases. The step disturbance is applied on the output (u_{vib} in Figure 11) to model a perturbation from the bottom stage of the mockup.

It is clearly shown that the linear controller designed neglecting the hysteresis effect leads to a strong overshoot (31%) and residual oscillations. On the contrary, using the nonlinear controller including the LIHO allows to efficiently overcome these issues. Practically, using the LIHO allows to linearize the response of the upper stage PEA, which leads to performances in line with the results presented in section "PI controller tuning."

Experimental results

The proposed approach has been tested on the experimental setup described in Figure 1. The experimental

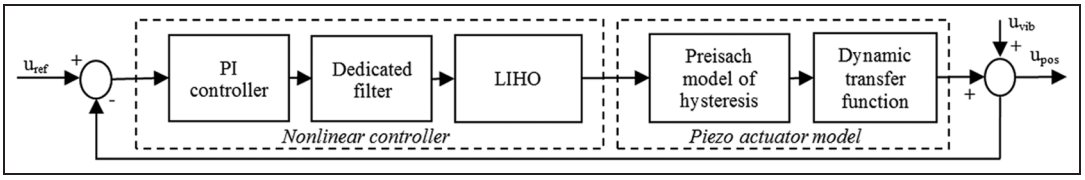

Figure 11. Block diagram of the closed-loop system.
LIHO: lightweight inverse hysteresis operator; PI: proportional–integral.

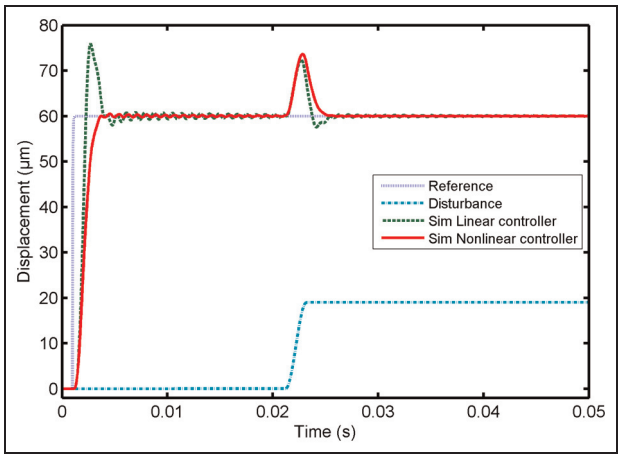

Figure 12. Simulated (SIM) 60-μm step response followed by a 20-μm step disturbance on the output.

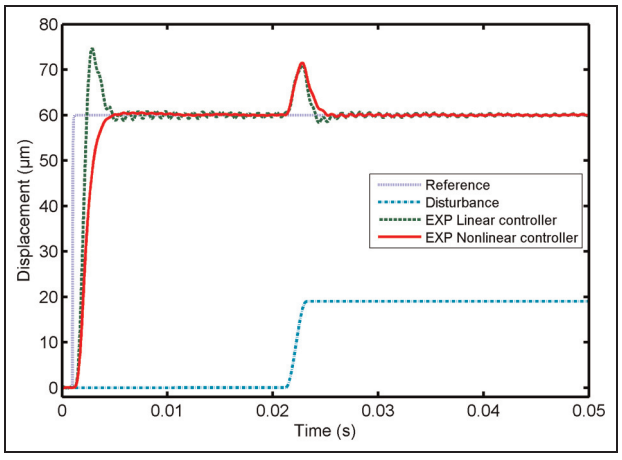

Figure 13. Experimental (EXP) 60-μm step response followed by a 20-μm step disturbance on the output.

closed-loop step responses using the linear controller (PI + filter) as well as the nonlinear controller (PI + filter + LIHO) are plotted in Figure 13. The controllers are implemented in the dSpace real-time system, with a 20-μs sample time. A step disturbance has been generated through APA_{vib} after 15 ms. The simulated responses plotted in Figure 12 are in very good agreement with the experimental results (absolute error is lower than 1 μm). Moreover, it is demonstrated that using the proposed nonlinear controller allows to get the ideal theoretical response depicted in Figure 8, which can be seen as a linearization of the actuator behavior.

The theoretical and experimental position tracking frequency responses are plotted in Figure 14. The theoretical response corresponds to the position tracking transfer function u_{pos}/u_{ref} plotted in Figure 9. The experimental data are obtained for a 40-μmpp (peak-to-peak displacement in micrometer) sinusoidal reference signal, whose frequency is changed step by step

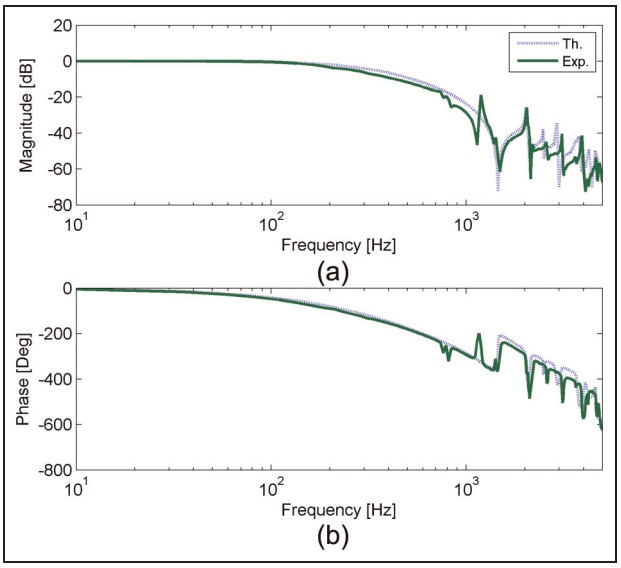

Figure 14. Comparison of theoretical (Th.) and experimental (EXP) position tracking frequency responses (u_{pos}/u_{ref}): (a) magnitude vs frequency and (b) phase vs frequency.

from 10 Hz to 5 kHz. No disturbance is generated by the APA_{vib} actuator. The position tracking gain is given by the ratio between the reference amplitude (u_{ref}) and the measured displacement amplitude (u_{pos}), and the phase is given by the phase difference between both displacements. A really good agreement is observed with discrepancies lower than 3 dB and 15° for frequencies lower than 500 Hz. Moreover, the frequency responses confirm that an effective tracking control of the position is obtained from DC to 190 Hz (−3 dB at 190 Hz).

The second objective of the proposed controller is to efficiently reject the disturbances due to ambient vibrations. The experimental and theoretical frequency responses of the output sensitivity are plotted in Figure 15. The theoretical curve corresponds to the u_{pos}/u_{vib} transfer function (also plotted as dashed line in Figure 9).

To get the experimental response, a 40 Vpp sinusoidal voltage is applied on the APA_{vib}. The experimental output sensitivity is obtained at a given frequency from the comparison of the displacement u_{pos} with and without control: The disturbance rejection gain is given by the ratio between the displacement amplitudes with and without control, and the phase is given by the phase difference between both displacements. The incremental evolution of the APA_{vib} frequency from 10 Hz to 5 kHz leads to the experimental output frequency response plotted in Figure 15. The theoretical and the experimental results are in excellent agreement, since discrepancies lower than 1.5 dB and 5° are observed for frequencies up to 2 kHz. Moreover, it is clearly shown that an efficient disturbance rejection is obtained from DC to 100 Hz (−3 dB at 100 Hz).

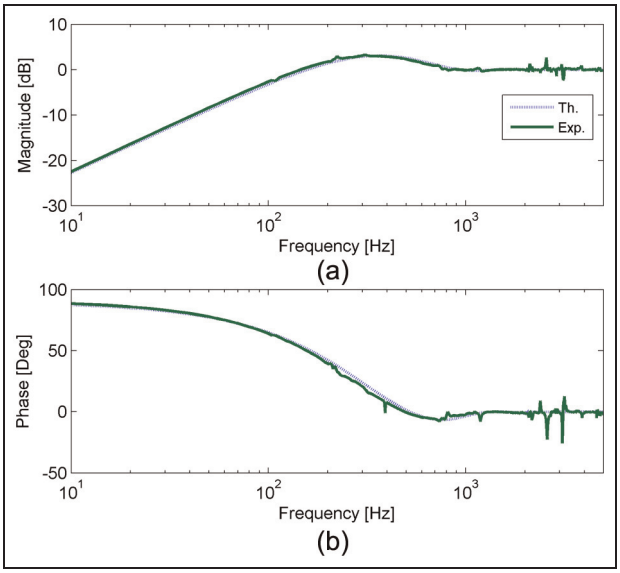

Figure 15. Comparison of theoretical (Th.) and experimental (EXP) output sensitivity frequency response (u_{pos}/u_{vib}): (a) magnitude vs frequency and (b) phase vs frequency.

Conclusion

A two-piezoelectric actuator stage experimental setup dedicated to the study of micropositioning and active isolation at the micrometer scale is presented. The bottom actuator is used to simulate the disturbances from ambient vibrations, whereas the upper stage is the positioning actuator itself, allowing a comprehensive study of both position tracking and disturbance rejection.

A control scheme is proposed. It combines a dedicated sixth-order filter, a PI controller and a LIHO used to linearize the actuator response. Linearization is usually performed using Preisach, GMS, Prandtl–Ishlinskii, or Bouc–Wen models.

It is demonstrated that the LIHO, combining high accuracy (asymmetric loops can be modeled) and simplicity (only six parameters), is a good alternative in the case of positioning close loop control.

The simulation and the experimental results present good performances in the frequency and time domains: The positioning settling time is about 2.56 ms, and the disturbances can be rejected up to 100 Hz. Moreover, it is demonstrated that the experimental results can be well anticipated by the theoretical approach, as long as the parameters are identified.

Funding

This work was financially supported by the French Ministry of Education and Research under the Pluri-Formation Program ViSta.

References

Badel A, Qiu J and Nakano T (2008a) A new simple asymmetric hysteresis operator and its application to inverse control of piezoelectric actuators. *IEEE Transactions on Ultrasonics, Ferroelectrics, and Frequency Control* 55(5): 1086–1094.

Badel A, Qiu J and Nakano T (2008b) Self-sensing force control of a piezoelectric actuator. *IEEE Transactions on Ultrasonics, Ferroelectrics, and Frequency Control* 55(12): 2571–2581. Available at: http://www.ncbi.nlm.nih.gov/pubmed/19126482

Badel A, Qiu J, Sebald G, et al. (2007) Self-sensing high speed controller for piezoelectric actuator. *Journal of Intelligent Material Systems and Structures* 19(3): 395–405. Available at: http://jim.sagepub.com/cgi/doi/10.1177/1045389X07083603

Cao Y and Yang B (2012) Non-linear modelling of multilayer piezoelectric actuators in non-trivial configurations based on actuator design parameters and piezoelectric material properties. *Journal of Intelligent Material Systems and Structures* 23(8): 875–884. Available at: http://jim.sagepub.com/cgi/doi/10.1177/1045389X12441508

Ge P and Jouaneh M (1995) Modeling hysteresis in piezoceramic actuators. *Precision Engineering* 17(3): 211–221. Available at: http://linkinghub.elsevier.com/retrieve/pii/014163599500002U

Goldfarb M and Celanovic N (1997) Modeling piezoelectric stack actuators for control of micromanipulation. *IEEE Control Systems Magazine* 17(3): 69–79. Available at: http://ieeexplore.ieee.org/xpls/abs_all.jsp?arnumber=588158

Jang M-J, Chen C-L and Lee J-R (2009) Modeling and control of a piezoelectric actuator driven system with asymmetric hysteresis. *Journal of the Franklin Institute* 346(1): 17–32. Available at: http://linkinghub.elsevier.com/retrieve/pii/S001600320800077X

Kuhnen K (2003) Modeling, identification and compensation of complex hysteretic nonlinearities a modified Prandtl-Ishlinskii approach. *European Journal of Control* 9(4): 407–418.

Kuhnen K and Janocha H (1999) Adaptive inverse control of piezoelectric actuators with hysteresis operators. In: *Proceedings of the European control conference ECC99*, Karlsruhe, Germany, pp. 1–6. Available at: http://klaus kuhnen.de/images/pdf/ECC99.pdf

Mayhan P, Srinivasan K, Watechagit S, et al. (2000) Dynamic modeling and controller design for a piezoelectric actuation system used for machine tool control. *Journal of Intelligent Material Systems and Structures* 11(10): 771–780. Available at: http://jim.sagepub.com/cgi/doi/10.1106/NVE7-PLK0-B96V-EUUL

Ninness B, Wills A and Gibson S (2005) The university of Newcastle identification toolbox (UNIT). In: *Proceedings of the IFAC World Congress*, Prague, Czech Republic, pp. 1–6. Available at: http://citeseerx.ist.psu.edu/viewdoc/download?doi=10.1.1.161.5537&;rep=rep1&type=pdf

Seo TW, Kim HS, Kang DS, et al. (2008) Gain-scheduled robust control of a novel 3-DOF micro parallel positioning platform via a dual stage servo system. *Mechatronics* 18(9): 495–505. Available at: http://linkinghub.elsevier.com/retrieve/pii/S0957415808000500

Shan Y and Leang KK (2012) Dual-stage repetitive control with Prandtl–Ishlinskii hysteresis inversion for piezo-based nanopositioning. *Mechatronics* 22(3): 271–281. Available at: http://linkinghub.elsevier.com/retrieve/pii/S0957415811001917

Song G, Zhao J, Zhou X, et al. (2005) Tracking control of a piezoceramic actuator with hysteresis compensation using inverse Preisach model. *IEEE/ASME Transactions on Mechatronics* 10(2): 198–209. Available at: http://ieeexplore.ieee.org/xpls/abs_all.jsp?arnumber=1420328

Song J and Der Kiureghian A (2006) Generalized Bouc-Wen model for highly asymmetric hysteresis. *Journal of Engineering Mechanics* 132(6): 610–618. Available at: http://escholarship.org/uc/item/4qk5c7vf

Trabia MB, Yim W and Saadeh M (2011) Modeling of hysteresis and backlash for a smart fin with a piezoelectric actuator. *Journal of Intelligent Material Systems and Structures* 22(11): 1161–1176. Available at: http://jim.sagepub.com/cgi/doi/10.1177/1045389X11414223

Wang DH, Zhu W and Yang Q (2010) Linearization of stack piezoelectric ceramic actuators based on Bouc-Wen model. *Journal of Intelligent Material Systems and Structures* 22(5): 401–413. Available at: http://jim.sagepub.com/cgi/doi/10.1177/1045389X10386132